IEEE Access
Multidisciplinary | Rapid Review | Open Access Journal

Received March 10, 2021, accepted March 24, 2021, date of publication March 29, 2021, date of current version April 6, 2021.

Digital Object Identifier 10.1109/ACCESS.2021.3069500

Non-Convex High Order Total Variation With Overlapping Group Sparsity Denoising Model Under Cauchy Noise

JIANGUANG ZHU[1], HAIJUN LV[1], BINBIN HAO[2], AND JIANWEN PENG[3]

[1]College of Mathematics and Systems Science, Shandong University of Science and Technology, Qingdao 266590, China
[2]College of Science, China University of Petroleum, Qingdao 266580, China
[3]School of Mathematical Sciences, Chongqing Normal University, Chongqing 400047, China

Corresponding author: Binbin Hao (bbhao981@163.com)

This work was supported in part by the Project of Shandong Province Higher Educational Science and Technology Program, China under Grant J17KA166, in part by the Major Program of the National Natural Science Foundation of China under Grant 11991024, in part by the Qindao Postdoctoral Science Foudation, China under Grant 2016114, and in part by the Science and Technology Support Plan for Youth Innovation of Colleges and Universities of Shandong Province of China under Grant 2019KJI005.

ABSTRACT It is widely known that the total variation regularization model preserves the edges well in the restored images but has some staircase effects. We consider using non-convex high-order total variation and overlapping group sparsity as a hybrid regularization to present a new denoising model. The proposed model can well preserve edges and reduce the staircase effect in the smooth region of the restored images. In order to solve the proposed hybrid model, we develop an efficient alternating minimization method. Compared with other models for removing Cauchy noise, numerical experimental results demonstrate that the superiority of the proposed model and algorithm, both in terms of visual and quantitative measures.

INDEX TERMS Non-convex high-order total variation, overlapping group sparsity, Cauchy noise.

I. INTRODUCTION

Image restoration mainly includes image denoising and deblurring, which is an important problem in image processing. We all known that image restoration is a typically linear inverse problem [1]. The objective of image restoration is to establish an appropriate image degradation model, and then make a reasonable estimate of the original image by solving the inverse problem. In mathematics, the image degradation model can be described as follows:

$$f = u + \tau, \tag{1}$$

where $u \in R^{n\times n}$ is the original image, f is the observed image, τ denotes the noise. The objective of noise reduction is to estimate the true clean image u from its noisy observation f. To deal with this problem, adding some regularization terms to energy is usually considered. Tikhonov regularization [2] is one of the commendable regularization method, where Tikhonov *et al.* use a quadric functional of the L_2 norm of the gradient magnitude $\|\nabla u\|$ i.e. $\|\nabla u\|_2^2$ as the regularization term. However, this model produces over-smoothness while removing noise. In order to overcome this drawback, Rudin *et al.* [3] proposed the following total variation (TV) regularization model(also known as ROF model)

$$\arg\min_u \frac{1}{2}\|u-f\|_2^2 + \lambda\|\nabla u\|_1,$$

where $\lambda > 0$ is a regularization parameter. Although the classical TV regularization model has the ability of preserving the edges, it also suffers from the well-known staircase artifacts. In order to reduce the staircase artifacts, one choice is using high-order total variation (HTV) [4], [5] as a regularization. Although HTV regularization can alleviate the staircase effect, it may reduce the ability of edges-preserving. More recently, Liu *et al.* proposed a new model using the overlapping group sparsity (OGS) regularization [6] to reduce staircase artifacts. By combining TV and HTV regularization, some hybrid regularization models are proposed [7], [8] to overcome the staircase effects and preserve edges simultaneously.

The above models have a good effect in processing Gaussian noise, but have poor processing ability for non-Gaussian noise, such as Rician noise, Gamma noise and Cauchy noise. In this paper, we focus on restoring images with Cauchy

The associate editor coordinating the review of this manuscript and approving it for publication was Yilun Shang.

noise, which usually appeared in radar and sonar, biomedical images, atmospheric and underwater acoustic [9]–[12]. In recent years, many methods have been proposed to remove Cauchy noise. In [13], Chang *et al.* considered an image restoration method with Cauchy noise based on the recursive recovery algorithm of Markov random field model. Achim *et al.* [14] removed Cauchy noise using a bivariate maximization posterior estimation in the complex wavelet domain. In [15], Wan *et al.* proposed a novel segmentation method for color images to remove Cauchy noise. Based on TV regularization and non-convex data-fidelity term, Mei *et al.* [16] proposed a non-convex model for Cauchy noise removal. Due to the nonconvexity and nonsmoothness of the proposed model, they developed a specific alternating direction method of multiplier to solve it. Although, they proved that their method converged to a stationary point, the restored results by their method strongly depends on the initializations. To overcome this disadvantage, Sciacchitano *et al.* [17] proposed the following convex variational model by adding a quadratic penalty function to the nonconvex data-fidelity term

$$\arg\min_u \frac{\alpha}{2}\left(\left\langle log\left(\gamma^2+(u-f)^2\right),\mathbf{1}\right\rangle_X+\mu\left\|u-u_0\right\|_F^2\right)+\left\|\nabla u\right\|_1, \quad (2)$$

where u_0 denotes the image obtained by applying the median filter to the noisy image f, $\langle\cdot,\cdot\rangle_X$ denotes the standard inner product, $\mathbf{1}$ is an $n\times n$ matrix of ones, $\mu>0, \alpha>0$ are the parameters. In order to reduce staircase artifacts and preserve edges, Yang *et al.* [18] replaced TV regularization in the model (2) by TV and HTV regularization and proposed a hybrid convex variational regularization model (''HTVAM'' for short). Moreover, they also introduced an efficient alternating minimization algorithm which can adaptively select regularization parameters. By combining total variation with overlapping group sparsity, Ding *et al.* [19] proposed the following convex variational model (''OGSTVL1'' for short) for eliminating Cauchy noise:

$$\arg\min_u \frac{\alpha}{2}\left(\left\langle log\left(\gamma^2+(u-f)^2\right),\mathbf{1}\right\rangle_X+\mu\left\|u-u_0\right\|_F^2\right)+\phi\left(\nabla u\right), \quad (3)$$

where, $\phi(\nabla u)$ is the OGS-TV regular function. They utilized the alternating direction method of multiplies(ADMM) and majorization minimization(MM) method to propose an efficient algorithm to solve the model (3). The numerical experiments showed that their method maintains the edge-preserving property of the TV method and overcomes staircase effects effectively.

On the other hands, the l_1 norm regularization terms in TV-based image restoration gives rise to over-smoothing problem. Compared with l_1 norm, l_p $(0<p<1)$ norm can measure sparsity better. In order to overcome this disadvantage, many non-convex l_p norm regularization are introduced. In [20], Chartrand first proposed a non-convex optimization problem using l_p norm as the objective function and he gave the theoretical l_p reconfigurable conditions for arbitrary sparse signals. In addition, Wen *et al.* [21] further theoretically demonstrated the superiority of the l_p norm-based method. In [22], Zhang *et al.* proved that non-convex l_p norm regularization in TV-based image restoration lead to even better edge preservation when compared to the convex l_1 norm regularization in their numerical experiments.

Motivated by the above studies, we propose the following hybrid model combining non-convex HTV and OGS-TV regularization for removing Cauchy noise:

$$\arg\min_u \frac{\alpha}{2}\left(\left\langle log\left(\gamma^2+(u-f)^2\right),\mathbf{1}\right\rangle_X+\mu\left\|u-u_0\right\|_F^2\right)+\omega\left\|\nabla^2 u\right\|_p^p+\phi(\nabla u), \quad (4)$$

where $\alpha>0, \mu>0$ and $\omega>0$ are regularization parameters, $p\in(0,1)$. To the best of our knowledge, this is the first time that non-convex HTV and OGS-TV regularization as a hybrid regularization term is considered for Cauchy noise. The main contributions of this paper are as follows:(1) We first combine non-convex HTV and OGS-TV regularization together in Cauchy noise removal model. This hybrid regularization model is beneficial to improve the OGS-TV sparsity and effectively remove the Cauchy noise in the degraded image. (2)Using the technique of variable substitution, we develop a new algorithm under the framework of alternating direction method of multipliers (ADMM) to solve the proposed model. (3)We conduct extensive experiments to demonstrate that our proposed method has superior performance over the state-of-the-art methods in Cauchy denoising. By adding OGS-TV term to non-convex l_p regularization, the edges and texture of the restored image are enhanced significantly. At the same time, this method greatly reduces the staircase artifacts caused by total variation.

The structure of the paper is as follows. In Section II, we give the definitions of second-order TV function and OGS-TV function. In Section III, we propose an efficient alternating minimization algorithm for solving the proposed model. In Section IV, we give some numerical results to demonstrate the effectiveness of the proposed model and algorithm. Finally, we conclude this paper in Section V.

II. PRELIMINARY

In this section, we introduce some preliminaries that will be used in this paper.

A. TOTAL VARIATION OF THE MATRIX

$u\in R^{n\times n}$ is a gray image. We introduce the following first-order forward and backward difference operators:

$$\left(\nabla_x^+ u\right)_{i,j}=\begin{cases}u_{i+1,j}-u_{i,j} & i<n,\\ u_{1,j}-u_{n,j} & i=n,\end{cases}$$

$$\left(\nabla_x^- u\right)_{i,j}=\begin{cases}u_{1,j}-u_{n,j} & i=1,\\ u_{i+1,j}-u_{i,j} & i>1,\end{cases}$$

$$\left(\nabla_y^+ u\right)_{i,j} = \begin{cases} u_{i,j+1} - u_{i,j} & j < n, \\ u_{i,1} - u_{i,n} & j = n, \end{cases}$$
$$\left(\nabla_y^- u\right)_{i,j} = \begin{cases} u_{i,1} - u_{i,n} & j = 1, \\ u_{i,j+1} - u_{i,j} & j > 1. \end{cases}$$

According to the above operators, we can defined the second-order difference operators as

$$\left(\nabla_{xx}^{-+} u\right)_{i,j} = \left(\nabla_x^- \left(\nabla_x^+ u\right)\right)_{i,j}, \quad \left(\nabla_{yy}^{-+} u\right)_{i,j} = \left(\nabla_y^- \left(\nabla_y^+ u\right)\right)_{i,j},$$
$$\left(\nabla_{xy}^{++} u\right)_{i,j} = \left(\nabla_y^+ \left(\nabla_x^+ u\right)\right)_{i,j}, \quad \left(\nabla_{yx}^{++} u\right)_{i,j} = \left(\nabla_x^+ \left(\nabla_y^+ u\right)\right)_{i,j},$$

where $u_{i,j}$ represents (i,j)th pixel in the image, $i,j = 1,\cdots,n$. Then, we can obtain the discrete TV and HTV of u as:

$$TV(u) = \|\nabla u\|_1 = \sum_{i,j} |(\nabla u)_{i,j}|,$$
$$HTV(u) = \|\nabla^2 u\|_1 = \sum_{i,j} |(\nabla^2 u)_{i,j}|,$$
$$\nabla^2 u = \begin{pmatrix} \nabla_{xx}^{-+} u & \nabla_{xy}^{++} u \\ \nabla_{yx}^{++} u & \nabla_{yy}^{-+} u \end{pmatrix}.$$

B. OGS-TV

For any vector $t \in R^n$, Selesenick and Chen [23] define a K-point group as

$$t_{i,K} = \{x(i), x(i+1), \cdots, x(i+K-1)\}.$$

And then, they use $t_{i,K}$ to define a group sparsity regularizer for one-dimensional case as

$$\varphi(t) = \sum_i \|t_{i,K}\|_2^2.$$

Similarly, for the two-dimensional image matrix $u \in \mathbb{R}^{n\times n}$, Liu [6] define a K-square-point group as

$$\widehat{u}(i,j)_K = \begin{pmatrix} u_{i-m_1,j-m_1} & \cdots & u_{i-m_1,j+m_2} \\ \vdots & \ddots & \vdots \\ u_{i+m_2,j-m_1} & \cdots & u_{i+m_2,j+m_2} \end{pmatrix} \in \mathbb{R}^{K\times K},$$

where $m_1 = \lfloor \frac{K-1}{2} \rfloor$, $m_2 = \lfloor \frac{K}{2} \rfloor$, $\lfloor x \rfloor$ denotes the largest integer not more than x. Arranging the $K \times K$ of $\widehat{u}(i,j)_K$ in lexicographic order, we obtain a vector $u(i,j)_K$. Then, we can defined the overlapping group sparsity functional of the two-dimensional array as

$$\varphi(u) = \sum_{i,j} \left\| u(i,j)_K \right\|_2. \tag{5}$$

Consequently, the regularization functional $\phi(\nabla u)$ in (3) can be given as:

$$\phi(\nabla u) = \varphi\left(\nabla_x^+ u\right) + \varphi\left(\nabla_y^+ u\right).$$

III. PROPOSED METHOD

In this section, we develop an efficient alternating minimization method to solve our proposed nonconvex model (4). By introducing three auxiliary variables t, q, w, the minimization problem (4) can be changed into the following equivalent form

$$\begin{aligned} &\arg\min_{u,z,v,q} \frac{\alpha}{2}\left(\left\langle log\left(\gamma^2 + (v-f)^2\right), \mathbf{1}\right\rangle_X + \mu\left\|v - u_0\right\|_F^2\right) \\ &+\omega \|q\|_p^p + \phi(z) \\ &s.t.\ z = \nabla u, q = \nabla^2 u, v = u \end{aligned} \tag{6}$$

Firstly, we define the following augmented Lagrangian function of (6):

$$\begin{aligned} &\mathcal{L}\left(u, z, v, q, \lambda_1, \lambda_2, \lambda_3\right) \\ &= \frac{\alpha}{2}\left(\left\langle log\left(\gamma^2 + (v-f)^2\right), \mathbf{1}\right\rangle_X + \mu\left\|v - u_0\right\|_F^2\right) \\ &+\omega\|q\|_p^p + \phi(z) + \frac{\beta_1}{2}\left\|z - \nabla u - \frac{\lambda_1}{\beta_1}\right\|_2^2 \\ &+\frac{\beta_2}{2}\left\|q - \nabla^2 u - \frac{\lambda_2}{\beta_2}\right\|_2^2 + \frac{\beta_3}{2}\left\|\text{v-u} - \frac{\lambda_3}{\beta_3}\right\|_2^2, \end{aligned} \tag{7}$$

where $\beta_1, \beta_2, \beta_3 > 0$ and $\lambda_i, i = 1,2,3$ are penalty parameter and the lagrange multipliers, respectively. Based on the classical ADMM, starting at $u = u^k, z = z^k, v = v^k, q = q^k$ and $\lambda_i = \lambda_i^k, i = 1,2,3$, the iterative scheme is implemented via the following subproblems:

$$\begin{cases} u^{k+1} \leftarrow \arg\min_u \mathcal{L}(u, z^k, v^k, q^k, \lambda_1^k, \lambda_2^k, \lambda_3^k), \\ z^{k+1} \leftarrow \arg\min_z \mathcal{L}(u^{k+1}, z, v^k, q^k, \lambda_1^k, \lambda_2^k, \lambda_3^k), \\ q^{k+1} \leftarrow \arg\min_q \mathcal{L}(u^{k+1}, z^{k+1}, v^k, q, \lambda_1^k, \lambda_2^k, \lambda_3^k), \\ v^{k+1} \leftarrow \arg\min_v \mathcal{L}(u^{k+1}, z^{k+1}, v, q^{k+1}, \lambda_1^k, \lambda_2^k, \lambda_3^k), \\ \lambda_1^{k+1} \leftarrow \lambda_1^k - \beta_1(z^{k+1} - \nabla u^{k+1}), \\ \lambda_2^{k+1} \leftarrow \lambda_2^k - \beta_2(q^{k+1} - \nabla^2 u^{k+1}), \\ \lambda_3^{k+1} \leftarrow \lambda_3^k - \beta_3(v^{k+1} - u^{k+1}). \end{cases} \tag{8}$$

In the following, we solve the subproblems in (8) in the detail.
(a) u-subproblem

$$\begin{aligned} &u^{k+1} \\ &= \arg\min_u \mathcal{L}\left(u, z^k, v^k, q^k, \lambda_1^k, \lambda_2^k, \lambda_3^k\right) \\ &= \arg\min_u \frac{\beta_1}{2}\left\|z^k - \nabla u - \frac{\lambda_1^k}{\beta_1}\right\|_2^2 + \frac{\beta_2}{2}\left\|q^k - \nabla^2 u - \frac{\lambda_2^k}{\beta_2}\right\|_2^2 \\ &\quad +\frac{\beta_3}{2}\left\|v^{\text{k-u}} - \frac{\lambda_3^k}{\beta_3}\right\|_2^2 \end{aligned} \tag{9}$$

By using the direct differential method, the Euler-Lagrange equation of (9)is given as follows:

$$\begin{aligned} &\left(\beta_1 \nabla^T \nabla + \beta_2 \left(\nabla^2\right)^T \nabla^2 + \beta_3 I\right) u^{k+1} \\ &= \beta_1 \nabla^T \left(z^k - \frac{\lambda_1^k}{\beta_1}\right) + \beta_2 (\nabla^2)^T \left(q^k - \frac{\lambda_2^k}{\beta_2}\right) \\ &\quad +\beta_3 \left(v^k - \frac{\lambda_3^k}{\beta_3}\right). \end{aligned} \tag{10}$$

Under the periodic boundary conditions for u, the solution of equation (10) can be obtained by using fast Fourier transform operation $\mathcal{F}$ and inverse fast Fourier operation $\mathcal{F}^{-1}$

$$u^{k+1} = \mathcal{F}^{-1}\Big(\frac{M}{\mathcal{F}\big(\beta_1\nabla^T\nabla + \beta_2(\nabla^2)^T\nabla^2 + \beta_3 I\big)}\Big), \quad (11)$$

where $M = \mathcal{F}\big(\beta_1\nabla^T(z^k - \frac{\lambda_1^k}{\beta_1}) + \beta_2(\nabla^2)^T(q^k - \frac{\lambda_2^k}{\beta_2}) + \beta_3(v^k - \frac{\lambda_3^k}{\beta_3})\big)$.

(b) z-subproblem

$$\begin{aligned} z^{k+1} &= \arg\min_z \mathcal{L}\left(u^{k+1}, z, v^k, q^k, \lambda_1^k, \lambda_2^k, \lambda_3^k\right) \\ &= \arg\min_z \frac{\beta_1}{2}\left\|z - \left(\nabla u^{k+1} + \frac{\lambda_1^k}{\beta_1}\right)\right\|_2^2 + \phi(z) \end{aligned} \quad (12)$$

It is easy to see that we can use majorization minimization (MM) method [6] to solve the problem (12).

(c) q-subproblem

$$\begin{aligned} q^{k+1} &= \arg\min_q \mathcal{L}\Big(u^{k+1}, z^{k+1}, v^k, q, \lambda_1^k, \lambda_2^k, \lambda_3^k\Big) \\ &= \arg\min_q \frac{\beta_2}{2}\left\|q - \left(\nabla^2 u^{k+1} + \frac{\lambda_2^k}{\beta_2}\right)\right\|_2^2 + \omega\|q\|_p^p \end{aligned} \quad (13)$$

In order to minimize problem (15), we use the iteratively re-weighted l_1 algorithm (IRL1) [24]. First, we use the similar strategies in [24] to approximate the l_p minimization problem (13) to the following weighted l_1 problem

$$q^{k+1} = \arg\min_q \frac{\beta_2}{2}\left\|q - \left(\nabla^2 u^{k+1} + \frac{\lambda_2^k}{\beta_2}\right)\right\|_2^2 + \sum_{i=1}\eta_i|q_i| \quad (14)$$

where the weight η_i is given by the following updating scheme

$$\eta_i = \frac{\omega p}{\left(|q_i^k| + \varepsilon\right)^{1-p}},$$

with ε being a small positive number to avoid division by zero. Let $x^{k+1} = \nabla^2 u^{k+1} + \frac{\lambda_2^k}{\beta_2}$, then minimization problem (14) can be given by one-dimensional shrinkage

$$q^{k+1} = \max\left\{|x^{k+1}| - \tfrac{\eta_i}{\beta_2}, 0\right\} \cdot sign\big(x^{k+1}\big). \quad (15)$$

(d) v-subproblem

$$\begin{aligned} v^{k+1} &= \arg\min_v \mathcal{L}\big(u^{k+1}, z^{k+1}, v, q^{k+1}, \lambda_1^k, \lambda_2^k, \lambda_3^k\big) \\ &= \arg\min_v \frac{\alpha}{2}\Big(\big\langle log\big(\gamma^2 + (v-f)^2\big), \mathbf{1}\big\rangle_X + \mu\big\|v - u_0\big\|_F^2\Big) \\ &\quad + \frac{\beta_3}{2}\left\|v - u^{k+1} - \frac{\lambda_3^k}{\beta_3}\right\|_2^2 \end{aligned} \quad (16)$$

If we denote

$$\begin{aligned} G(v) = \frac{\alpha}{2}\Big(\big\langle log\big(\gamma^2 + (v-f)^2\big), \mathbf{1}\big\rangle_X + \mu\big\|v - u_0\big\|_F^2\Big) \\ + \frac{\beta_3}{2}\left\|v - u^{k+1} - \frac{\lambda_3^k}{\beta_3}\right\|_2^2, \end{aligned}$$

The gradient and Hessian matrices of $G(v)$ are given by the following equations,

$$\begin{aligned} G'(v) &= \frac{\alpha(v-f)}{\gamma^2 + (v-f)^2} + \alpha\mu\big(v - u_0\big) \\ &\quad + \beta_3\big(v - u^{k+1}\big) - \beta_3\lambda_3^k, \\ G''(v) &= \frac{\alpha(\gamma^2 - (v-f)^2)}{(\gamma^2 + (v-f)^2)^2} + \alpha\mu + \beta_3. \end{aligned}$$

The solution of problem (16) can be obtained by Newton's method

$$v^{k+1,l+1} = v^{k+1,l} - \frac{G'(v^{k+1,l})}{G''(v^{k+1,l})}, \quad (17)$$

where $k+1$ and $l+1$ are the numbers of outer iteration and Newton iteration, respectively.

(e) Updating multipliers via $\lambda_1, \lambda_2, \lambda_3$

Finally, three Lagrange multipliers in (8) are updated as follows:

$$\begin{aligned} \lambda_1^{k+1} &= \lambda_1^k - \beta_1\big(z^{k+1} - \nabla u^{k+1}\big), \\ \lambda_2^{k+1} &= \lambda_2^k - \beta_2\big(q^{k+1} - \nabla^2 u^{k+1}\big), \\ \lambda_3^{k+1} &= \lambda_3^k - \beta_3\big(v^{k+1} - u^{k+1}\big). \end{aligned} \quad (18)$$

The whole algorithm for removing Cauchy noise is given in Algorithm 1.

Algorithm 1 The Proposed Method for Solving Model (4)

Initialize $u^0 = f$, v, q, z, ω, Group size K, Max iteration N, $\alpha > 0$, $\lambda_1^0, \lambda_2^0, \lambda_3^0$, $k = 0$, the number of iterations of MM algorithm *Nit-inner*,

1. **While** "not converged", **Do**
2. Compute u^{k+1} according to (11);
3. Compute z^{k+1} according to (12);
4. Compute q^{k+1} according to (15);
5. Compute v^{k+1} according to (17);
6. Update λ_i^{k+1}, i = 1,2,3 according to (18);
7. **End Do**
8. Output u.

IV. EXPERIMENTS AND DISCUSSION

In this section, we present several numerical results to demonstrate the effectiveness of the proposed model and method. All test images are shown in FIGURE 1, which are gray images with the size of 256 × 256. All the numerical experiments are implemented under Windows 10 and Matlab R2018a running on a laptop equipped with 2.60 GHz Inter(R) Core(TM) i5-3230M and 4GB memory.

A. EXPERIMENT SETTING

In the following experiments, we use the following degradation equation to generate the noisy image f

$$f = u + \tau = u + \xi\frac{\tau_1}{\tau_2}.$$

where $\xi > 0$ represents the noise level, τ_1 and τ_2 are independent random variables and follow from the Gaussian

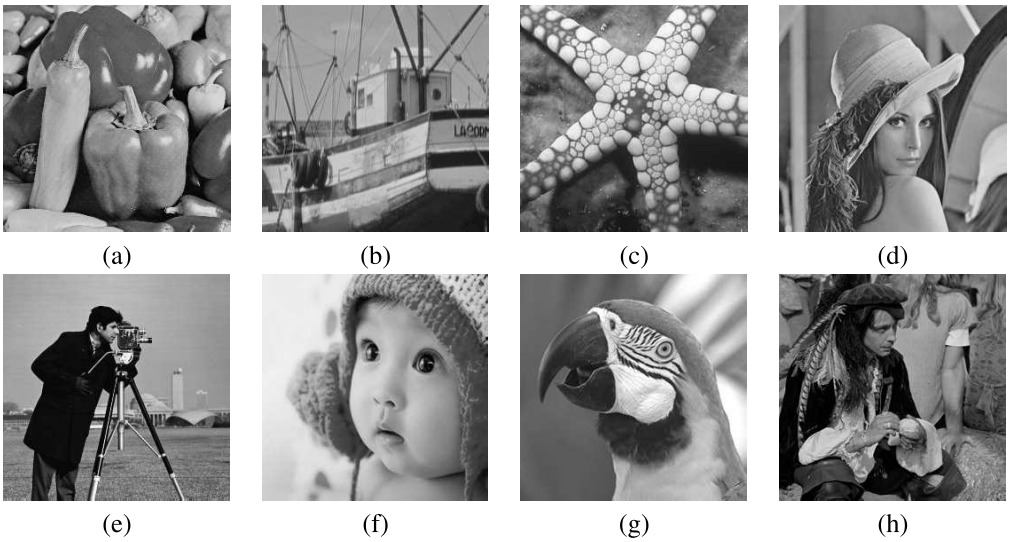

FIGURE 1. Test images: (a) Peppers, (b) Boats, (c) Starfish, (d) Lena, (e) Cameraman, (f) Babyface, (g) Parrots, (h) Man.

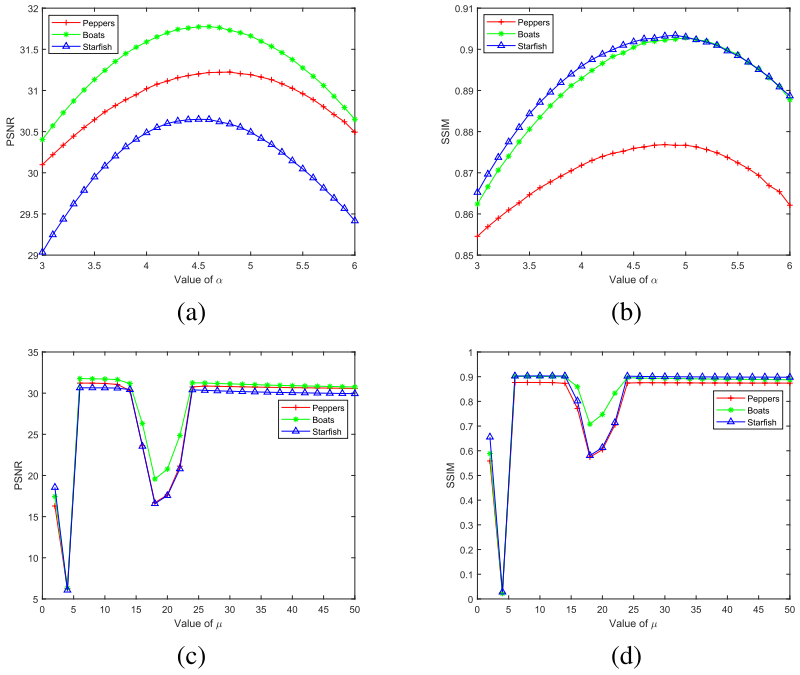

FIGURE 2. Top row: the PSNR and SSIM values with respect to the regularization parameter α. Bottom row: the PSNR and SSIM values with respect to the parameter μ.

distribution with mean 0 and variance 1. It is the same as the parameter setting in [19], we set $\gamma = \sqrt{\xi}$ for all the experiments in this paper.

The peak signal-to-noise (PSNR) and the structural similarity index measurement (SSIM) are used to measure the quality of the restored images. The PSNR is given by the following formulation:

$$PSNR = 10\log_{10}\frac{255^2}{\frac{1}{n^2}\|u-\widetilde{u}\|_2^2},$$

where u and $\widetilde{u}$ are the ideal image and the recovered image, respectively. Generally, the larger PSNR values imply that the restored images are better. The SSIM [25] is defined as follows:

$$SSIM = \frac{(2\mu_u\mu_{\widetilde{u}} + C_1)(2\sigma_{u\widetilde{u}} + C_2)}{(\mu_u^2 + \mu_{\widetilde{u}}^2 + C_1)(\sigma_u^2 + \sigma_{\widetilde{u}}^2 + C_2)},$$

where μ_u, $\mu_{\widetilde{u}}$, σ_u and $\sigma_{\widetilde{u}}$ represent the mean values and the standard variance of images u and $\widetilde{u}$, $\sigma_{u\widetilde{u}}$ is the covariance of u and $\widetilde{u}$, C_1 and C_2 are two positive constants. Note that

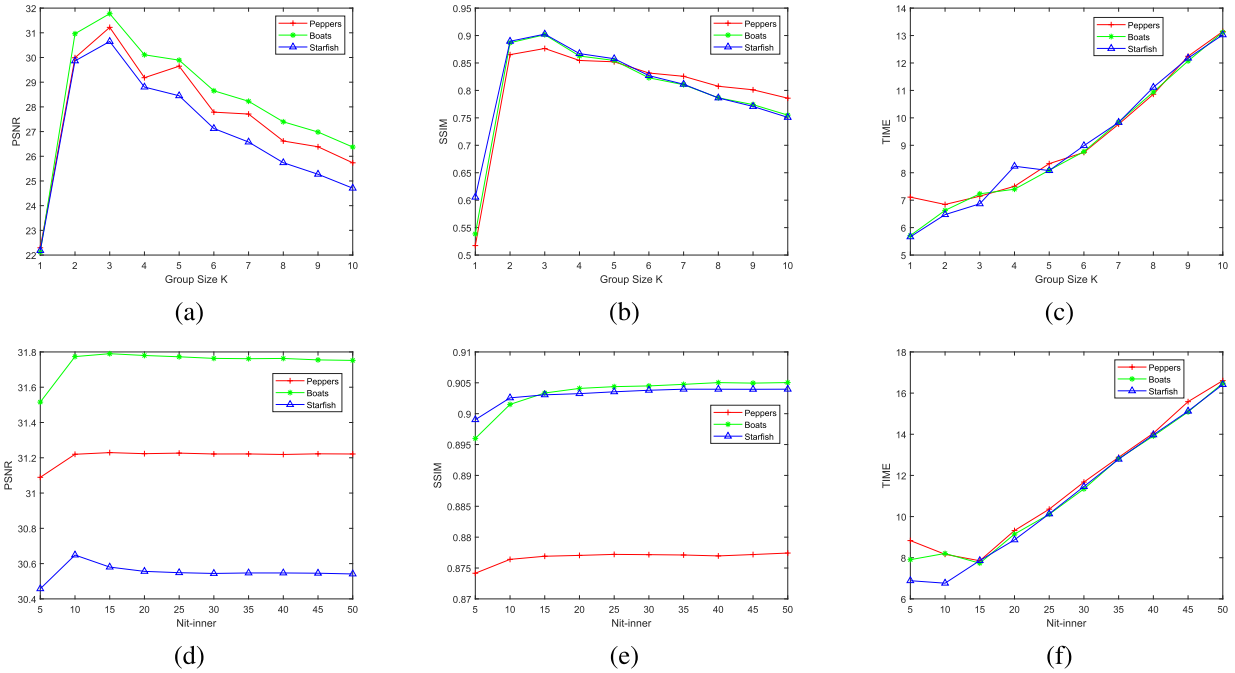

FIGURE 3. Top row: the PSNR, SSIM and CPU time values with respect to the Group Size K. Bottom row: the PSNR, SSIM and CPU time values with respect to the number of iterations *Nit-inner*.

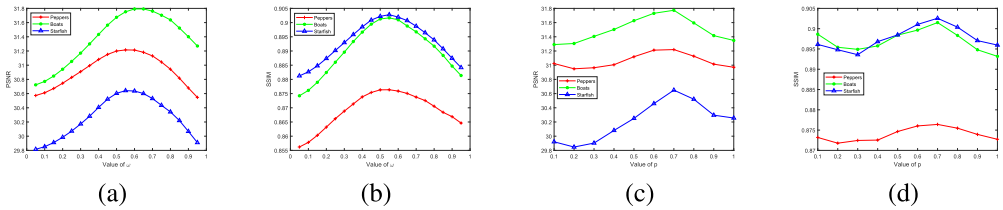

FIGURE 4. The PSNR and SSIM values with respect to ω, p.

SSIM is between 0 and 1, if the values of SSIM is closer to 1, the features of the restored images are similar to the original image.

The stopping criterion for all of the tested algorithms was set to

$$\frac{\left\|u^{k+1}-u^{k}\right\|_F}{\left\|u^{k}\right\|_F}<10^{-5},$$

where u^k is the restored image in the k-th iteration. Throughout all the experiments, we set the penalty parameters $\beta_1 = 30, \beta_2 = 2.5, \beta_3 = 10$ for the noise level $\xi = 0.02$; and $\beta_1 = 50$, $\beta_2 = 9.5$, $\beta_3 = 10$ for the noise level $\xi = 0.04$.

B. PARAMETER DISCUSSION

In this subsection, we show how to select the best values for parameters $\alpha, \mu, \omega, p, K$, *Nit-inner* for different test images. The images "Peppers", "Boats" and "Starfish" are used to study the choice of these parameters. Cauchy noise with the noise level $\xi = 0.02$ is added into these three tested images.

In order to find out how the parameters α and μ impact the performance of our proposed method. We first fix other parameters and let α to vary continuously from 3 to 6. Next, we use the same method to tune the parameter μ. The changes of PSNRs and SSIMs versus different values of parameters α and μ in FIGURE 2. It is easy to see that the performance of the proposed method achieves the best with α in 4.5 nearby. We set $\alpha = 4.6$ in the following experiments. It can also be observed that the maximum values of PSNR and SSIM are obtained when the parameter $\mu \in [6, 12]$ and $\mu > 25$. From FIGURE 2, we can observe that the values of PSNR and SSIM are stable when $\mu > 25$. However, the calculation time increases with the increase of μ. Then, in the following experiments, we set $\mu = 6$.

Next, we test how to select a good value of the group size K and the number of MM inner iterations *Nit-inner*. We carry out experiments to compute the values of PSNR, SSIM, CPU Times with respect to K and *Nit-inner*. From FIGURE 3, we can see that the highest PSNR and SSIM values are obtained at $K = 3$. Therefore,

FIGURE 5. Denoising results of three methods at $\xi = 0.02$. First column : Noisy images; second column : Restored image by OGSTVL1 method third column : Restored image by HTVAM method last column : Restored image by our method.

we choose $K = 3$ for in the following experiments. From FIGURE 3, we can also observe that the values of PSNR and SSIM tend to be stable when the iteration number *Nit-inner* ≥ 10, increasing the MM iteration *Nit-inner* does not dramatically effect the PSNR, SSIM, but, the algorithm takes more time. Therefore, we set *Nit-inner* $= 10$ in our experiments.

Finally, we plot the values of PSNR and SSIM obtained by our algorithm against different values of parameters ω, p in FIGURE 4. It can be observed that that the highest PSNR and SSIM values are obtained when $\omega = 0.57$, $p \in (0.6, 0.8)$. Then we empirically choose $\omega = 0.57$, $p = 0.7$, in the following experiments.

C. DENOISING

To demonstrate the superior performance of the proposed method, we compare it with other two state-of-the-art methods: OGSTVL1 [19] and HTVAM [18].

Experiment 1: We corrupt the images(as shown in FIGURE 1) adding Cauchy noise with the noise level $\xi = 0.02$. FIGURE 5 shows the denoising results by three different methods. It is not difficult to see that our proposed method outperforms the others in terms of both noise removal and detail preservation. To intuitively compare the local details of the restored images, we enlarged the red box region of images in FIGURE 5. Comparing to OGSTVL1 and HTVAM, our proposed method can preserve details and edges very well in

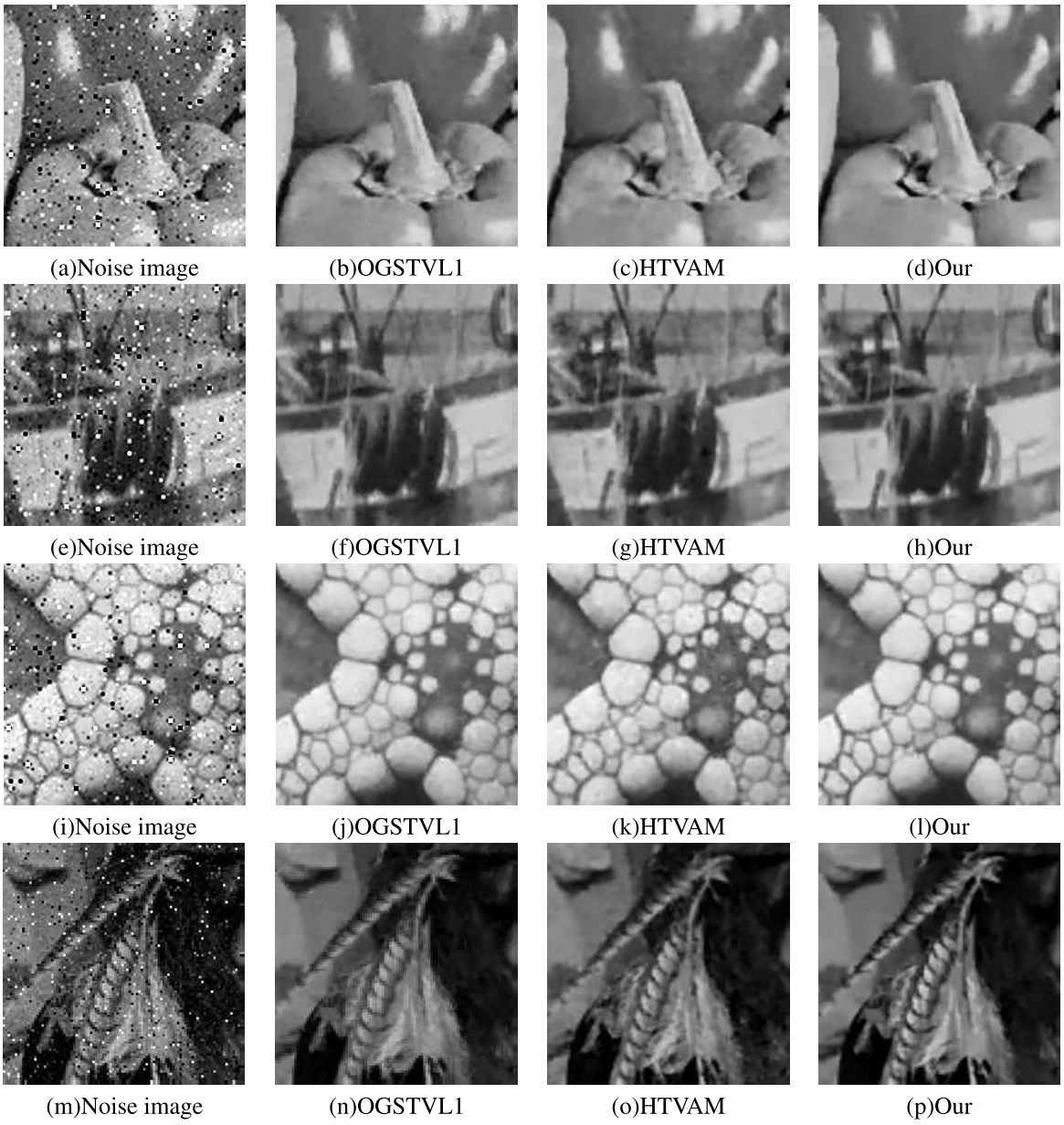

FIGURE 6. The zoomed regions of the recovered images in FIGURE 5. First column : Noisy images; second column : Restored images by OGSTVL1 method; third column : Restored images by HTVAM method; last column : Restored images by our method.

the restored images while removing most of the noisy pixels. In TABLE 1, we lists the values of PSNR and SSIM for the restored images by different methods. It is easy to see that the values of PSNR and SSIM for the restored images by our method are higher than the other two methods. It is consistent with the visual comparison. Moreover, our proposed method needs less time than the other two methods. Then we conclude that our proposed method behaves much better than the other two methods.

Experiment 2: We restore the images ''Babyface'', ''Lena'' by three different methods under the noise level $\xi = 0.04$. The restored images are shown in FIGURE 7. In order to illustrate the differences between the restoration given by different methods, we shows the zoomed regions of the recovered images in FIGURE 8. From the recovered images, it is easy to see that the HTVAM method and OGSTVL1 method yields staircase artifacts in the denoising results, while our proposed method overcomes this drawback. The restored image obtained by the algorithm in this paper is closer to the original image, and the smoothness of the local area is more prominent. We also report the values of PSNR and SSIM obtained by these three methods in TABLE 2. From the table, we observe that our proposed method can get better restoration results than the other two methods, in terms of

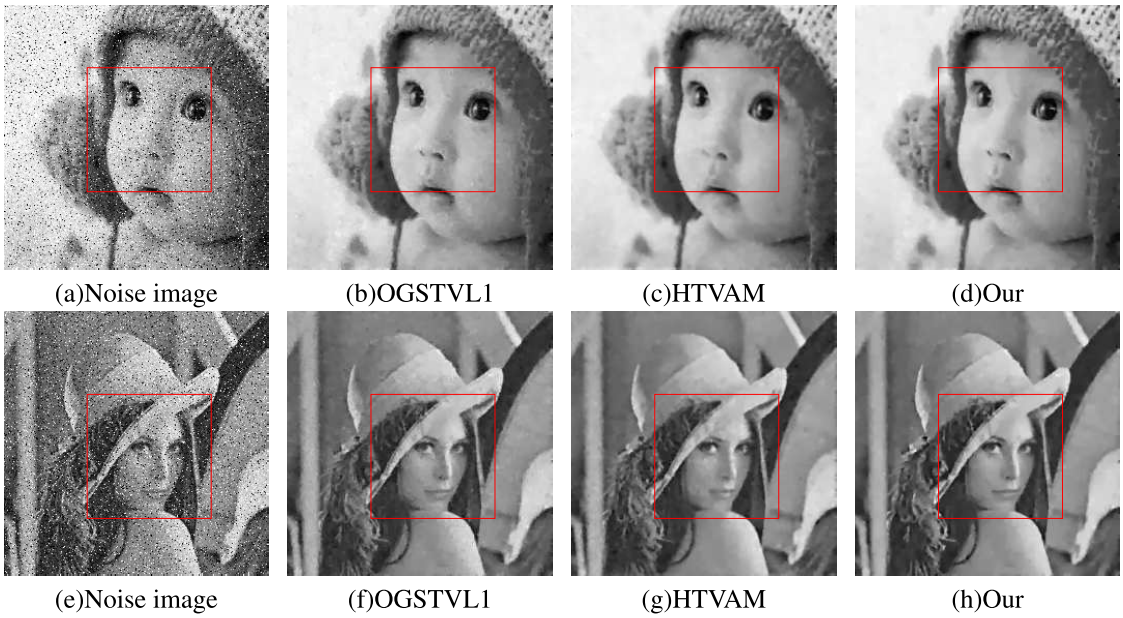

FIGURE 7. Denoising results of three methods at $\xi = 0.04$. First column : Noisy images; second column : Restored image by OGSTVL1 method third column: Restored image by HTVAM method last column : Restored image by our method.

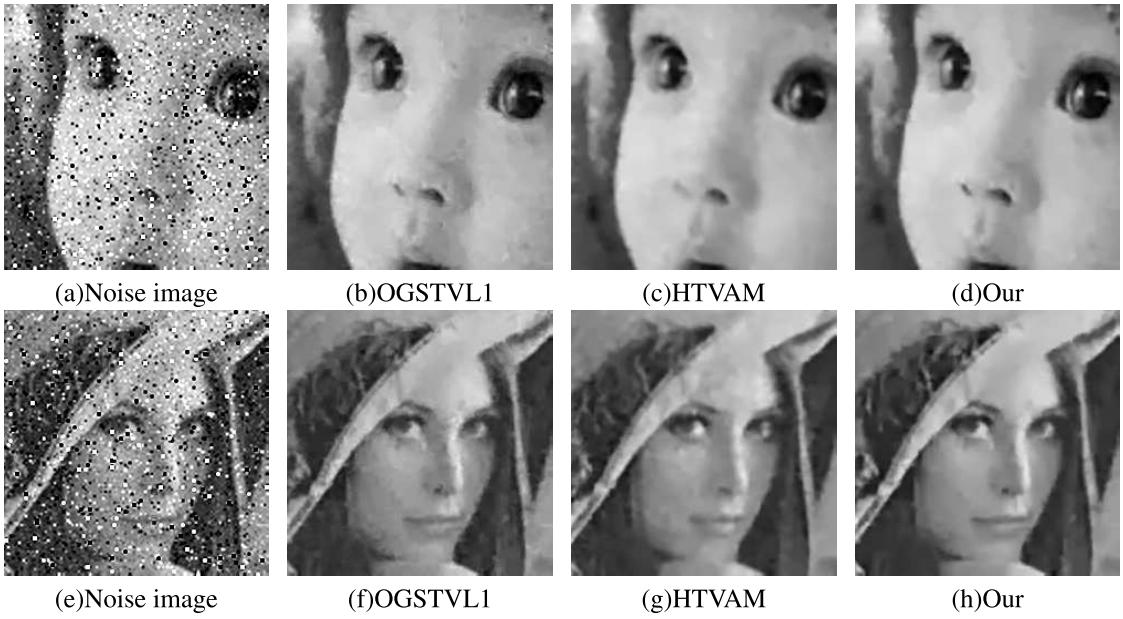

FIGURE 8. The zoomed regions of the recovered images in FIGURE 7. First column : Noisy images; second column : Restored image by OGSTVL1 method; third column : Restored image by HTVAM method; last column : Restored image by our method.

the PSNRs and SSIMs. From FIGURES 7,8, and TABLE 2, we conclude that our proposed method behaves better than the HTVAM method and OGSTVL1 method.

D. THE CONVERGENCE OF THE PROPOSED METHOD

In this subsection, we plot the convergence curve to verify the convergence of our proposed methods experimentally. Here, we tested six images of ''Peppers'', ''Boats'', ''Lena'', ''Babyface'', ''Parrots'' and ''Man'' degraded by Cauchy noise with the noise level $\xi = 0.02$ and $\xi = 0.04$. The values of PSNR, SSIM and Relative error versus iteration numbers are presented in FIGURE 9. From FIGURE 9, It is not difficult to see that the curves of PSNR value, SSIM value and the Relative Error value are flat when the number of iterations increases a certain value.

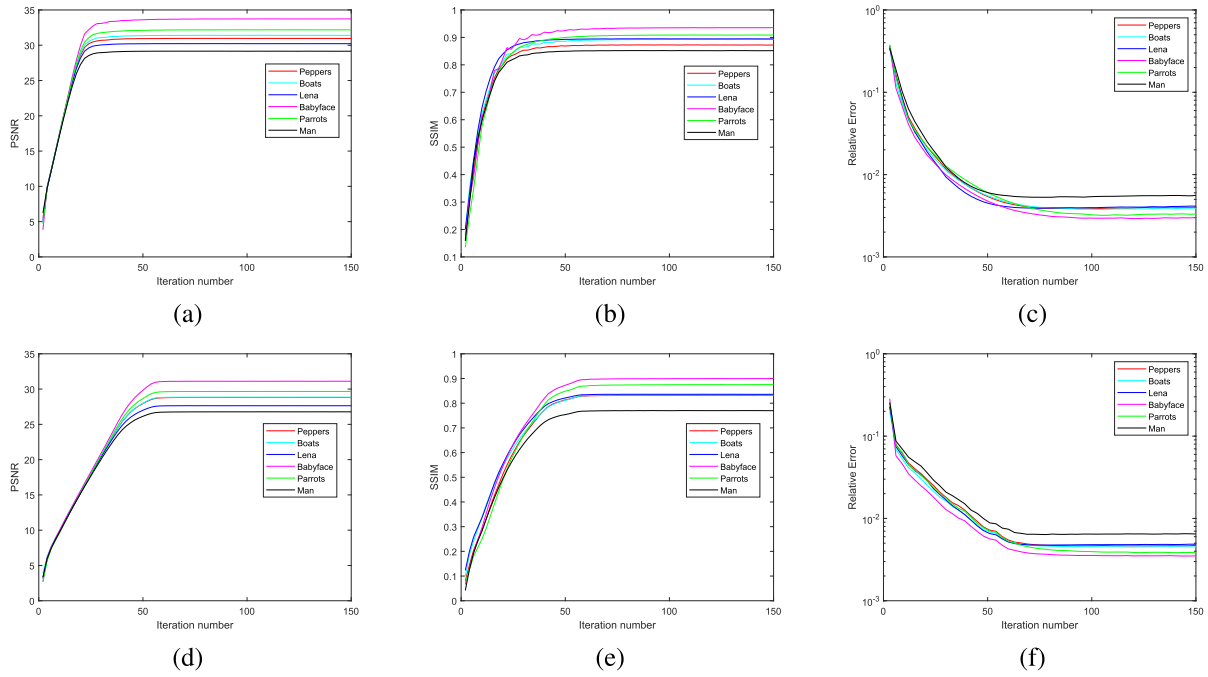

FIGURE 9. Top row: the convergence of the proposed method versus the iteration numbers with the noise level $\xi = 0.02$. Bottom row: the convergence of the proposed method versus the iteration numbers for different images with the noise level $\xi = 0.04$.

TABLE 1. The values of PSNR and SSIM for different methods ($\xi = 0.02$).

Images		Ours	OGSTVL1	HTVAM
Pepper	PSNR(dB)	**31.2290**	30.3404	30.7226
	SSIM	**0.8767**	0.8719	0.8665
Boats	PSNR(dB)	**31.7945**	30.1372	31.2259
	SSIM	**0.9022**	0.8920	0.8908
Starfish	PSNR(dB)	**30.6422**	30.0669	30.2067
	SSIM	**0.9030**	0.8932	0.8943
Lena	PSNR(dB)	**32.0149**	31.4359	31.6814
	SSIM	**0.9118**	0.8999	0.9038
Cameraman	PSNR(dB)	29.0423	28.9313	**29.1165**
	SSIM	**0.8806**	0.8781	0.8702
Babyface	PSNR(dB)	**33.9404**	33.3374	33.6115
	SSIM	**0.9393**	0.9328	0.9369
Parrots	PSNR(dB)	**32.5790**	32.0530	32.2845
	SSIM	**0.9119**	0.9032	0.9147
Man	PSNR(dB)	**29.6039**	29.2867	29.4276
	SSIM	**0.8669**	0.8634	0.8641

TABLE 2. The values of PSNR and SSIM for different methods ($\xi = 0.04$).

Images		Ours	OGSTVL1	HTVAM
Pepper	PSNR(dB)	**29.1650**	27.9332	28.4963
	SSIM	**0.8385**	0.8197	0.8269
Boats	PSNR(dB)	**29.2929**	27.7217	28.7900
	SSIM	**0.8486**	0.8305	0.8354
Lena	PSNR(dB)	**29.5119**	29.0254	29.2057
	SSIM	**0.8674**	0.8429	0.8589
Babyface	PSNR(dB)	**31.4022**	30.6917	30.7418
	SSIM	**0.9044**	0.8704	0.9002
Parrots	PSNR(dB)	**30.1393**	29.6286	29.9543
	SSIM	**0.8780**	0.8525	0.8813
Man	PSNR(dB)	**27.3248**	27.1220	27.1775
	SSIM	**0.7946**	0.7915	0.7899

V. CONCLUSION

In this paper, we proposed a new Cauchy noise removal model by combining nonconvex l_p norm regularization with OGS-TV regularization. The proposed model inherited the advantage of both the HTV and OGS-TV to effectively reduce the stair casing artifacts while preserving sharp edges well. Based on ADMM method, IRL1 method and MM algorithm, we developed an efficient alternating minimization algorithm. Numerical results demonstrated that the proposed model and method performed better both quantitatively and qualitatively.

ACKNOWLEDGMENT

The authors would like to thank Meng Ding and Jinghua Yang of the University of Electronic Science and Technology of China for generously sharing the codes for OGSTVL1 and HTVAM with them.

REFERENCES

[1] J. Hadamard, "Sur les problèms aux dérivées partielles et leur signification physique," *Princeton Univ. Bull.*, vol. 13, pp. 49–52, 1902.
[2] A. N. Tikhonov and V. Y. Arsenin, "Solutions of ill-posed problems," *Math. Comput.*, vol. 32, no. 144, p. 491, 1977.
[3] L. I. Rudin, S. Osher, and E. Fatemi, "Nonlinear total variation based noise removal algorithms," *Phys. D, Nonlinear Phenomena*, vol. 60, nos. 1–4, pp. 259–268, Nov. 1992.
[4] T. Chan, A. Marquina, and P. Mulet, "High-order total variation-based image restoration," *SIAM J. Sci. Comput.*, vol. 22, no. 2, pp. 503–516, Jan. 2000.
[5] M. Lysaker, A. Lundervold, and X.-C. Tai, "Noise removal using fourth-order partial differential equation with applications to medical magnetic resonance images in space and time," *IEEE Trans. Image Process.*, vol. 12, no. 12, pp. 1579–1590, Dec. 2003.
[6] G. Liu, T.-Z. Huang, J. Liu, and X.-G. Lv, "Total variation with overlapping group sparsity for image deblurring under impulse noise," *PLoS ONE*, vol. 10, no. 4, Apr. 2015, Art. no. e0122562.
[7] F. Li, C. Shen, J. Fan, and C. Shen, "Image restoration combining a total variational filter and a fourth-order filter," *J. Vis. Commun. Image Represent.*, vol. 18, no. 4, pp. 322–330, Aug. 2007.

[8] M. Lysaker and X.-C. Tai, "Iterative image restoration combining total variation minimization and a second-order functional," *Int. J. Comput. Vis.*, vol. 66, no. 1, pp. 5–18, Jan. 2006.

[9] T. Pander, "New polynomial approach to myriad filter computation," *Signal Process.*, vol. 90, no. 6, pp. 1991–2001, Jun. 2010.

[10] M. Idan and J. L. Speyer, "Cauchy estimation for linear scalar systems," *IEEE Trans. Autom. Control*, vol. 55, no. 6, pp. 1329–1342, Jun. 2010.

[11] E. E. Kuruoglu, W. J. Fitzgerald, and P. J. W. Rayner, "Near optimal detection of signals in impulsive noise modeled with a symmetric α-stable distribution," *IEEE Commun. Lett.*, vol. 2, no. 10, pp. 282–284, Oct. 1998.

[12] G. Samoradnitsky, M. S. Taqqu, and R. Line, "Stable non-Gaussian random processes: Stochastic models with infinite variance," *Bull. London Math. Soc.*, vol. 28, no. 134, pp. 554–555, 1996.

[13] Y.-C. Chang, S. R. Kadaba, P. C. Doerschuk, and S. B. Gelfand, "Image restoration using recursive Markov random field models driven by cauchy distributed noise," *IEEE Signal Process. Lett.*, vol. 8, no. 3, pp. 65–66, Mar. 2001.

[14] A. Achim and E. E. Kuruoglu, "Image denoising using bivariate α-stable distributions in the complex wavelet domain," *IEEE Signal Process. Lett.*, vol. 12, no. 1, pp. 17–20, Jan. 2005.

[15] T. Wan, N. Canagarajah, and A. Achim, "Segmentation of noisy colour images using cauchy distribution in the complex wavelet domain," *IET Image Process.*, vol. 5, no. 2, p-. 159–170, 2011.

[16] J.-J. Mei, Y. Dong, T.-Z. Huang, and W. Yin, "Cauchy noise removal by nonconvex ADMM with convergence guarantees," *J. Sci. Comput.*, vol. 74, no. 2, pp. 743–766, Feb. 2018.

[17] F. Sciacchitano, Y. Dong, and T. Zeng, "Variational approach for restoring blurred images with cauchy noise," *SIAM J. Imag. Sci.*, vol. 8, no. 3, pp. 1894–1922, Jan. 2015.

[18] J.-H. Yang, X.-L. Zhao, J.-J. Mei, S. Wang, T.-H. Ma, and T.-Z. Huang, "Total variation and high-order total variation adaptive model for restoring blurred images with cauchy noise," *Comput. Math. Appl.*, vol. 77, no. 5, pp. 1255–1272, Mar. 2019.

[19] M. Ding, T.-Z. Huang, S. Wang, J.-J. Mei, and X.-L. Zhao, "Total variation with overlapping group sparsity for deblurring images under cauchy noise," *Appl. Math. Comput.*, vol. 341, pp. 128–147, Jan. 2019.

[20] R. Chartrand, "Exact reconstruction of sparse signals via nonconvex minimization," *IEEE Signal Process. Lett.*, vol. 14, no. 10, pp. 707–710, Oct. 2007.

[21] J. M. Wen, D. F. Li, and F. M. Zhu, "Stable recovery of sparse signals via l_p minimization," *Appl. Comput. Harmon. Anal.*, vol. 38, no. 1, pp. 161–176, 2015.

[22] H. Zhang, L. Wang, B. Yan, L. Li, A. Cai, and G. Hu, "Constrained total generalized p-variation minimization for few-view X-ray computed tomography image reconstruction," *PLoS ONE*, vol. 11, no. 2, Feb. 2016, Art. no. e0149899.

[23] I. W. Selesnick and P.-Y. Chen, "Total variation denoising with overlapping group sparsity," in *Proc. IEEE Int. Conf. Acoust., Speech Signal Process.*, May 2013, pp. 5696–5700.

[24] Q. Lyu, Z. Lin, Y. She, and C. Zhang, "A comparison of typical l_p minimization algorithms," *Neurocomputing*, vol. 119, no. 16, pp. 413–424, Nov. 2013.

[25] Z. Wang, A. C. Bovik, H. R. Sheikh, and E. P. Simoncelli, "Image quality assessment: From error visibility to structural similarity," *IEEE Trans. Image Process.*, vol. 13, no. 4, pp. 600–612, Apr. 2004.

JIANGUANG ZHU received the Ph.D. degree in applied mathematics from Xidian University, Xián, China, in 2011. He is currently an Associate Professor with the Shandong University of Science and Technology. His current research interests include optimization theory, algorithms and applications in image processing, and sparse representation.

HAIJUN LV received the B.S. degree in information and computing science from Dezhou University, Dezhou, China, in 2017. He is currently pursuing the M.S. degree with the Shandong University of Science and Technology. His research interests include image restoration and sparse optimization.

BINBIN HAO received the Ph.D. degree in applied mathematics from Xidian University, Xián, China, in 2010. In 2009, she joined the College of Science, China University of Petroleum, where she has been an Associate Professor, since 2012. Her current research interests include image processing, pattern recognition, wavelet analysis, and sparse representation.

JIANWEN PENG received the Ph.D. degree in applied mathematics from Inner Mongolia University, Hohhot, China, in 2005. In 2001, he served as an Associate Professor with the School of Mathematics, Chongqing Normal University, where he has been a Professor, since 2005. From November 2015 to November 2016, he was a Visiting scholar of Chinese Scholarship Council, The University of Minnesota, USA. His research interests include vector optimization, nonlinear programming, variational inequalities, equilibrium problems, generalized convexity and generalized monotonicity, and set-valued analysis.